Optical Microscopy Techniques Based On the Use of A Computer-controlled Hemispherical Digital Condenser

by

Dongyu Cao

B.Sc. in Physics

A Thesis

In

Applied Physics

Submitted to the Graduate Faculty
of Texas Tech University in
Partial Fulfillment of
the Requirements for
the Degree of

MASTERS OF SCIENCES

Approved

Dr. Luis Grave de Peralta
Chair of Committee

Dr. Ayrton Bernussi

Mark Sheridan
Dean of the Graduate School

December, 2015

ACKNOWLEDGMENTS

I would like to thank my research advisor, Dr. Luis Grave de Peralta, and Dr. Ayrton Bernussi from Nano Tech Center for the most help and support on my research. I would also like to thank everybody in our research group for the excellent collaboration on our project.

TABLE OF CONTENTS

ABSTRACT

A computer-controlled hemispherical digital condenser is presented in this work, and also a single device is demonstrated to be used to implement a variety of both well-established and novel optical microscopy techniques. In addition, condenser capabilities are verified by imaging fabricated periodic patterned structures and biological samples.

LIST OF FIGURES

CHAPTER I

INTRODUCTION

The minimum lateral image resolution that can be achieved with conventional optical microscopes is ~200 nm. These microscopes are often used in biomedical imaging applications because the dimensions of most cells are larger than this resolution limit. Frequently, a microscope condenser must be attached to the optical microscope in order to achieve such a resolution [1-3]. Microscope condensers enhance the resolution of the image by illuminating the sample with a cone of light [3]. A well-known consequence of this approach is that the minimum observable period with the microscope decreases from $p_{min} \sim \lambda/NA_o$ for a microscope without a condenser [4-6] to the well-known Rayleigh resolution limit of diffraction-limited imaging instruments $p_{min} \sim \lambda/(2NA_o)$ [1-7] when a condenser is used [1-3, 7]. Here, λ corresponds to the wavelength of the illumination source in vacuum, and NA_o is the numerical aperture of the microscope objective lens. Traditional microscope condensers consist of a combination of bulky lenses (or mirrors) and diaphragms designed to illuminate the sample with a cone of inclined light [3]. However, due to the demonstrated utility of microscope condensers, alternative methods to produce highly inclined illumination have been proposed to overcome some of the limitations of traditional microscope condensers. Recently developed plasmonic ultrathin condensers (UTC), with a volume three orders of magnitude smaller than bulky condensers [8-13], have a great potential for biomedical applications where a compact high-resolution imaging systems are needed [12]. Deep sub-wavelength resolution has been recently demonstrated using hemispherical [7] and planar [14-16] digital condensers with no lenses, mirrors or moving parts. Digital condensers illuminate the sample from multiple directions with inclined light produced by an array of light emitting diodes (LEDs). It has been demonstrated that a very flexible microscope condenser can be implemented using a planar array of LEDs, where each LED can be independently switched ON and OFF [14-16]. Such an electronically controlled

condenser permits a smooth switch from bright field to dark field microscopy without having to mechanically change the microscope condenser attached to the microscope or introducing a spatial filter in the back focal plane of the objective lens [14]. Moreover, electronically controlled microscope condensers permit to implement novel microscopy techniques providing resolution values well below the Rayleigh resolution limit of diffraction-limited imaging instruments [14-16]. Such condensers will find multiple applications in digital pathology, hematology, immunohistochemestry, and neuroanatomy [15]. However, a planar array of LEDs does not have the best geometry for implementing a microscope condenser because the distance of each LED to the sample is not constant [16]. Recently, hemispherical digital condensers (HDC) have been demonstrated [7] but without the capability to independently control each LED [16]. We anticipate that a computer-controlled HDC with this these characteristics will find multiple applications in FPM [16] and in other optical imaging techniques where controlled illumination from multiple directions is needed [17-18]. For instance, a multi-angle lensfree holographic imaging platform was demonstrated using three LEDs illuminating micro-particles on a chip from one vertical and two oblique angles [18]. In this work we report for the first time the development of a HDC where the ON/OFF state of each LED can be computer controlled [19]. The condenser characteristics are verified by imaging fabricated periodic structures and biological samples. The versatility of planar digital condensers has been previously demonstrated [14, 20-21]. It is demonstrated that a single computer-controlled HDC can also be used to implement a variety of both well-established and novel optical microscopy techniques. Moreover, we propose an alternative method for the numerical reconstruction of the synthetic FP image [22-23] often calculated in Fourier Ptychographic Microscopy (FPM) techniques [15].

CHAPTER II
DESCRIPTION OF THE EXPERIMENTS

Figure 1(a) illustrates the experimental set up used in the experiments. For obtaining the Real Plane (RP) and Fourier Plane (FP) images of the object under observation, a Nikon Eclipse Ti inverted microscope, objective lenses with different numerical apertures (NA_o) and magnifications, and two charge-coupled device (CCD) cameras are used. Band-pass spectral filters (BPF) centered at different wavelengths with a bandwidth of 10 nm may be inserted in the back focal plane (BFP) of the microscope objective lens. In all experiments described here the microscope's built-in white-light illumination source was substituted by the HDC, photograph of which is shown in Fig. 1(b). Each one of the 64 LEDs in the HDC with a hemisphere radius of 1.5 cm can be independently turned ON/OFF. A dedicate software was developed to control the individual LEDs of the HDC. The electronic hardware includes a 24-channel digital input/output device, two 8-channels source drivers, and a power supply [19]. This is shown in Figs. 1(b) and 1(c) where four different groups of LEDs were turned ON. As it is shown in Fig. 1(a), the HDC was placed directly on the top of the sample. The HDC was centered on the area of interest of the sample to be imaged and this was verified by taking the corresponding FP image. The emission spectrum of the white LEDs used in our experiments is shown in Fig. 1(d). The peak emission occurs at $\lambda\sim$ 450 nm, a weaker but broader secondary emission peak occur at $\lambda\sim$ 570 nm. Periodic Cr pillars structures with square lattice symmetry, period p, and pillar diameter $d=p/2$ are fabricated to obtain a quantitative evaluation of the resolution of the obtained RP images.

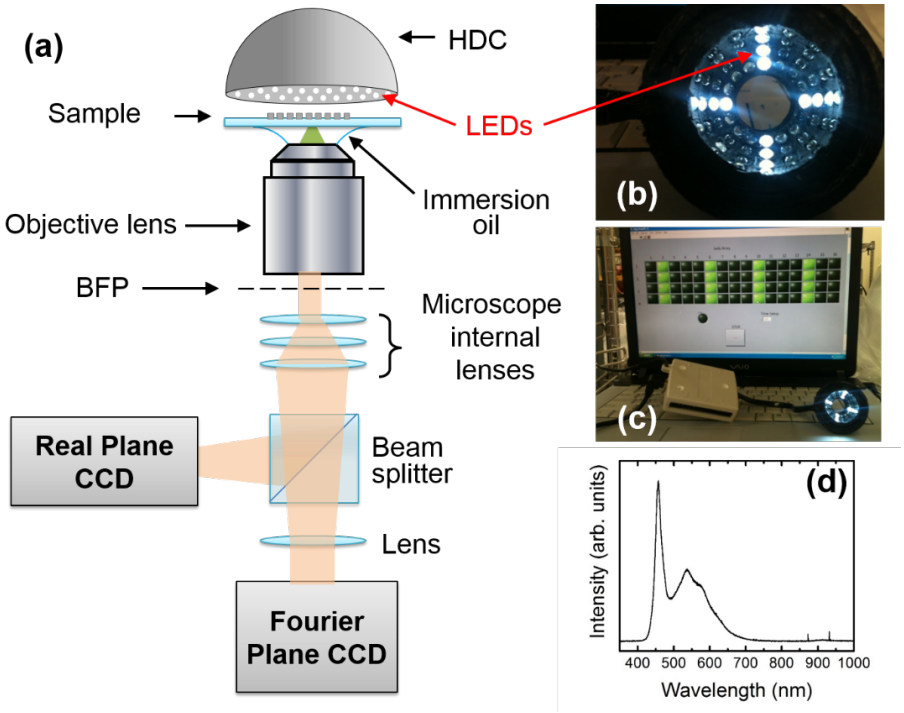

Fig. 1. (a) Schematic illustration of our experimental set up, (b) photograph of the HDC, and (c) associated electronic and computer. (d) LEDs emission spectrum.

In addition, living biological samples were also imaged. The Cr square lattice structures were fabricated by first spin coating a layer of PMMA, which serve as the patterning resist for e-beam lithography, which was defined over a 150 μm thick coverslip. A ~10 nm thick Al layer was thermally evaporated on top of the PMMA layer to provide a grounding element for the lithography process. After the lithography step, hydrofluoric acid (HF) was used to etch away the Al layer, and a methyl-isobutyl-ketone: isopropanol solution was used to develop the PMMA thereby revealing holes in the PMMA layer arranged in a square lattice pattern. A 15 nm thick Cr layer was then deposited on top of the PMMA layer, which filled in the holes in the square lattice arrangement, previously revealed. Finally, the sample was dipped in acetone to dissolve the PMMA layer thereby leaving only a periodic structure forming by Cr pillars which had adhered to the glass substrate (Fig. 2(b)).

CHAPTER III

EXPERIMENTAL RESULTS AND DISCUSSION

Figures 2(a) and 2(b) show FP and RP images, respectively, corresponding to a Cr pillar array with d=400 nm. The five dashed-line circumferences overlapping the FP image were introduced for helping to understand the features presented in the image. The images were obtained using the band-pass filter centered at λ=570 nm, and a 100× objective lens with NA_o=1.3, and only turning to the "ON" state all the LEDs corresponding to a single latitude of the HDC.

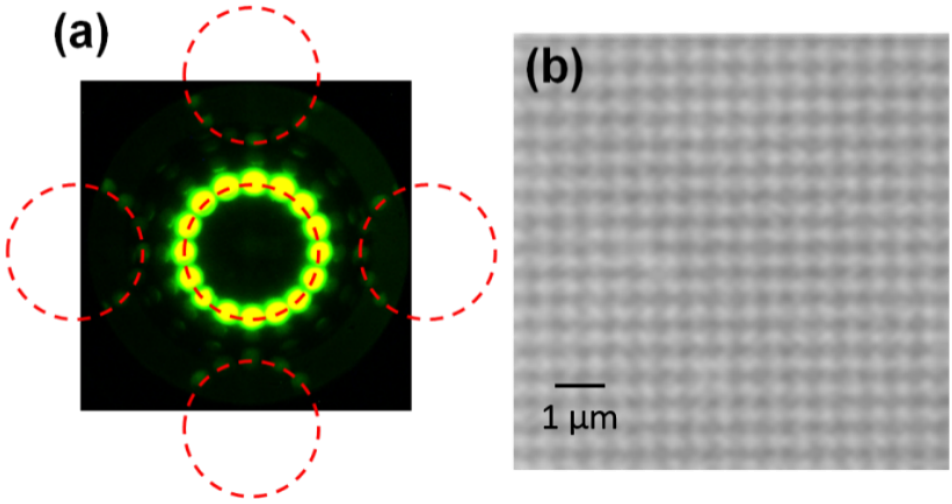

Fig. 2. (a) FP and (b) RP images of Cr pillars with p=400 nm obtained using a band-pass filter centered at λ=570 nm, NA_O=1.3, and only turning ON all the LEDs contained in a single latitude of the HDC.

The central bright ring observed in the FP image shown in Fig. 2(a) is the signature of the presence of a microscope condenser [8-13]. The four portions of rings in the FP shown in Fig. 2(a) correspond to the first-order diffraction rings produced by illuminating the Cr array with square symmetry with the light produced by the HDC [8-13]. The clear observation of the Cr array lattice in the RP image shown in Fig. 2(b) is in excellent correspondence with the observation of the zero-order and portions of the first-order diffraction rings in the FP image [9]. From the FP image we determined

NA_c~0.55 for the numerical aperture of the condenser [10]. As it is shown in Fig. 3 the NA_c can be simply varied by turning ON the LEDs in different latitudes of the HDC.

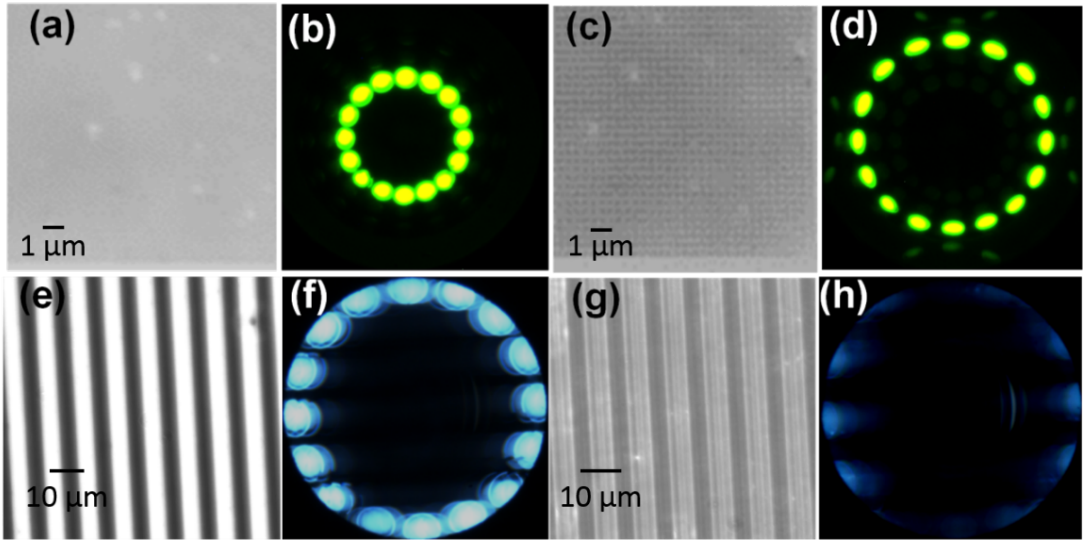

Fig. 3. (a), (c), (e), (g) RP and (b), (d), (f), (h) corresponding FP images of (a), (c) a Cr pillars array with p=300 nm and (e), (g) a Ronchi ruling target with a p=10 μm. The images were obtained using the HDC, a microscope objective lens with (a)-(d) NA_o=1.3 and (e)-(h) NA_o=0.65, and (e)-(h) without a band-pass filter but (a)-(d) with a band-pass filter cantered at λ=570 nm.

The images shown in Figs. 3(a) to 3(d) were obtained using the HDC, a band-pass filter centered at λ=570 nm, and 100× microscope objective lens with NA_o=1.3. The numerical aperture values corresponding to the central ring in the FP images shown in Fig. 3(b) and 3(d) are NA_c~0.55 and 0.89, respectively. Small fractions of the first-order diffraction rings are observed in the FP image shown in Figs. 3(d) but not in the FP shown in Fig. 3(b). There is an excellent agreement with this observation and the Abbe description of image formation in a microscope. Using a condenser [7, 9] the lattice structure of the sample is observed in the corresponding RP image shown in Figs. 3(c) but it is not observed in the RP image shown in Fig. 3(a). This is also in good correspondence with the known expression, which provides the minimum observable period using a condenser attached to a common optical microscope [1-2, 7]:

$$p_{\min} = \frac{\lambda}{NA_o + NA_c} \tag{1}$$

Using the experimental conditions described above, p_{min} = 308 nm and 260 nm are determined by Eq. (1) for NA_c =0.55 and 0.89, respectively; therefore, as it is confirmed by the images shown in Figs. 3(a) and 3(c), Eq. (1) predicts that the fabricated structure with p=300 nm should be visible when NA_c =0.89 but not when NA_c =0.55. As it is shown in the Figs. 3(e) to 3(h), the reconfigurable capability of changing NA_c in the HDC, also permits a smooth transition from obtaining bright-field to dark-field images of the object under observation. The images shown in Figs. 3(e) to 3(h) correspond to a Ronchi ruling with a period p=10 μm. They were obtained using the HDC, without a spectral filter, and a microscope a 40X objective lens with NA_o=0.65. The presence of a fraction the zero-order diffraction ring with NA_c ~0.55 in the FP image shown in Fig. 3(f) demonstrates that the RP image shown in Fig. 3(e) is a bright-field image of a commercial Ronchi ruling target. The RP image shown in Fig. 3(g) is a dark-field image of the same object, which was obtained by changing NA_c from 0.55 to 0.89. Consequently, as it is shown in the FP image shown in Fig. 3(h), only high-order diffraction rings were collected by the microscope objective lens. This resulted in the observation of more grove details in the RP image shown in Fig. 3(g) when compared with the one shown in Fig. 3(e).

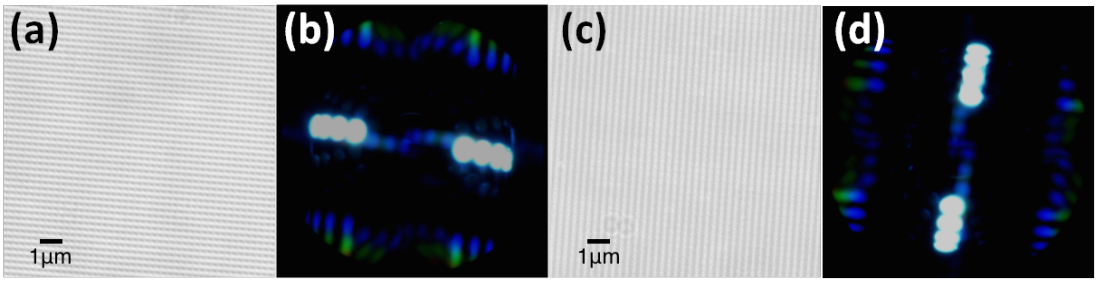

Fig. 4. (a), (c) RP and (b), (d) FP images of Cr pillars square array lattice with p=500 nm obtained using the HDC, and a microscope 100 × objective lens with NA_o=1.3. No band-pass filter was used in these experiments.

A computer-controlled HDC permits to illuminate the sample in a variety of configurations. Fig. 4 shows images of a square lattice array of Cr pillars with p=500 nm illuminated at different directions. As it has been previously reported [24], changing the illumination direction (Figs. 4(b) and 4(d)) permits to select horizontal (or vertical) Cr pillar lines (Figs. 4(a) and 4(c)) of the photonic crystal periodic array.

No band-pass filter was used to obtain the images shown in Fig. 4. Therefore, first-order diffraction maxima corresponding to the two spectral peaks of the LEDs emission (Fig. 1(d)) are clearly observed in the FP images shown in Figs. 4(b) and 4(d). However, no chromatic distortions are observable in the RP images shown in Figs. 4(a) and 4(c). The Rayleigh resolution limit of diffraction-limited imaging instruments can be obtained from in Eq. (1) when $NA_c = NA_o$. Nevertheless, it has been demonstrated that values of p_{min} much smaller than the Rayleigh resolution limit can be obtained when $NA_c >> NA_o$ using a microscope condenser and the Fourier plane imaging microscopy (FPIM) technique [9, 13], or using a digital condenser and the FPM technique [15]. FPM requires acquisition of multiple RP images, taken with a different individual LED in the ON state for each RP image [15-16]. As it is demonstrated by the images shown in Fig. 5, the computer-controlled HDC described in this work has this capability. The images of Cr pillars array with p= 500 nm were obtained using the HDC with a single LED in the ON state, a band-pass filter centered at λ=570 nm and a 100× microscope objective lens with NA_o=1.3.

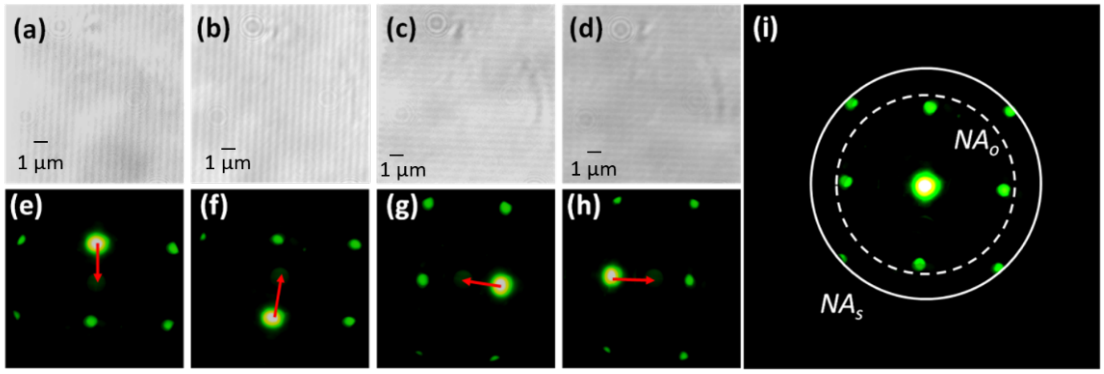

Fig. 5. (a)-(d) RP and (e)-(h) corresponding FP images of Cr pillars array with p=500 nm obtained using the HDC with a single LED in the ON state, a band-pass filter centered at λ=570 nm, and NA_o=1.3. (i) Synthetic FP image with $NA_s > NA_o$.

The FP images shown in Figs. 5(e) to 5(h) display the intensity distribution in the microscope's FP. They are formed by spots distributed with the same square lattice symmetry of the Cr array patterned in the sample. This indicates that the light illuminating the sample, which is emitted by a single LED, can be approximately described by a plane wave [6, 15-16]. The brightest spot in the FP image corresponds

to the zero-order diffraction spot; therefore, the spatial orientation and the phase of the incident plane wave can be in a simple way obtained from the position of the zero-order diffraction spot in the FP [6]. The FP image is basically the fraction of the Fourier transform of the periodic sample structure which is captured by the microscope objective lens; consequently, several high-order diffraction spots, arranged in square symmetry with a period $\Lambda=2\pi/p$ are observed in the FP images shown in Figs. 5(e) to 5(h). The number of these spots and their relative position with respect to the center of the FP image changes when the position of the single LED in the ON state changes. As it is shown in Fig. 5(i), a synthetic FP image with a numerical aperture $NA_s > NA_c$ can be constructed by the simple procedure of first shifting all the obtained FP images until the zero-order diffraction spots occupy the center of the FP image, followed by the sum of the shifted FP images. The necessary shift is indicated in Figs. 5(e) to 5(h) by the arrows pointing to the center of the low intensity small disk located at the center of the FP field of view of the microscope objective lens. The low intensity small disk observed in the FP images shown in Figs. 5(e) to 5(h) were formed by the portion of the white-light beam emitted by the microscope built-in illumination source passing through the center circular aperture of the HDC (see HDC photograph in Fig. 1(b)). In order to illustrate the concept, the synthetic FP image shown in Fig. 5(i) was simply obtained by adding the intensities of the shifted FP images; however, the phase of the synthetic optical disturbance [6, 22-23] at the FP could be calculated by implementing algorithms of phase recovery like in FPM [15-16, 25]. The starting point in FPM are multiple RP images corresponding to different illumination angles, then the synthetic optical disturbance at the FP is constructed using the numerical Fourier transform of each RP image [15-16]. However, in the method proposed in this work the starting point is the synthetic FP image shown in Fig. 5(i); therefore, a different phase recovery algorithm should be used. For instance, some iterative algorithms have been reported that permit to recover the phase from the intensity distribution recorded in a FP image [26]. The important point here is that similarly to FPM [15-16] and FPIM [9, 13], once the adequate phase recovery algorithm is implemented, a RP image with increased resolution should be obtained

because $NA_s > NA_c$. It is worth noting that this procedure may be simpler and faster than the one used in FPM. Therefore, a detailed development and implementation of the proposed algorithm of image reconstruction are expected to image living biological structures in real life by using computer-controlled HDCs.

CHAPTER IV
OBSERVATION OF BIOLOGICAL SAMPLES USING HDCS

In order to verify the applicability of the computer-controlled HDC for biomedical optical imaging, high quality images with improved resolution of unicellular organism are obtained by using the experimental set up, which are illustrated in Fig. 1(a).

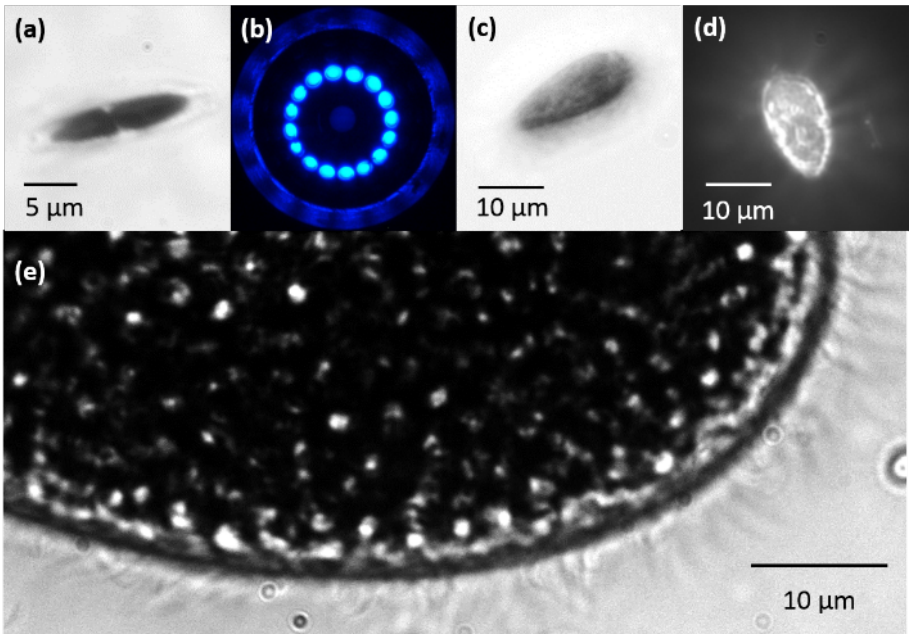

Fig. 6. (a) RP image (100 ×, NA_o=1.3) of a Diatom cell; (b) FP image of a Diatom cell (100 ×, NA_o=1.3); (c) Bright field image of a Euglena using (40 ×, NA_o= 0.65); (d) Dark field image of a Euglena using (40×, NA_o= 0.65); (e) RP image of Paramecium (100 ×, NA_o=1.3, all LEDs in the ON-state). The links show the RP (Media 1) and FP (Media 2) videos of a Paramecium using the computer-controlled HDC.

Figure 6 shows images of a collection of live single cell organisms of various sizes and shapes. Figure 6(a) shows the RP of a Diatom cell using a 100× microscope objective with NA_o=1.3 along with the HDC with only one latitude of LED ON having NA_c ~ 0.55. Figure 6 (b) shows the corresponding FP of 6(a). Figure 6(b) has only the zero order of illumination visible as the RP is a non-periodic structure. The outermost bright disc present in this FP image is due to the presence of water in the diatom solution. This diatom cell was obtained from a sample of mixed diatoms which

has a wide range of sizes and shapes. The valve of the diatom present at its center is of the order of 500 nm, it is possible to resolve this valve with the use of the HDC. Figure 6(c) and 6(d) shows bright and dark field images of Euglena bacteria using a NA_o=0.65 40× microscope objective lens with NA_c~0.55 and NA_c~0.77 respectively. Typical dimensions of Euglena ranges from 25-100 μm and this agrees with the dimensions obtained in our image. Figures 6(c) and 6(d) shows a smooth transition from bright to dark field microscopy without changing the microscope objective. Figure 6(e) shows a RP image of Paramecium bursaria which ranges from 80-150 μm and has hair like (cilia) structures of width of about 200 nm. The cilia was clearly resolved with the 100× microscope objective with NA_o=1.3 with all the LEDs of the HDC in the ON state. A real time video of this paramecium and consequently all the motions of the algae symbiotically living inside the paramecium have been included in the experiment. A FP video of the same paramecium moving across the field of view can also be photographed with the better resolution.

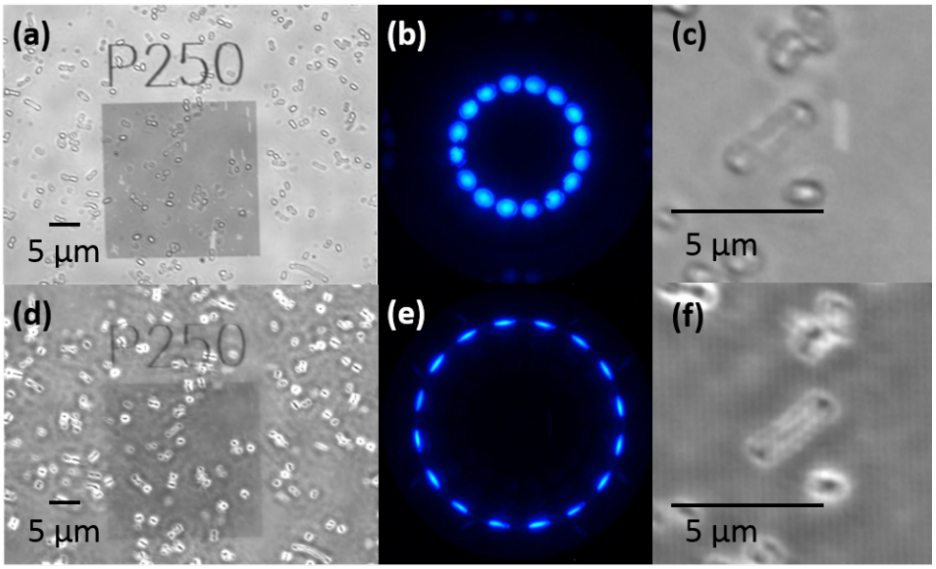

Fig. 7. (a), (c) RP and (b), (e) FP images of E. Coli obtained using the HDC, a band-pass filter centered at λ=450 nm, and NA_o=1.3. (c) and (f) were obtained by zooming in the RP images shown in (a) and (d), respectively.

Figure 7 shows the application of the HDC as a variable NA_c condenser using the images of E. Coli bacteria on a Cr square lattice array with p=250. A small amount of a water solution with living E. Coli bacteria was placed on a coverslip where a Cr

pillar array with p=250 nm was previously fabricated. E. Coli bacteria are clearly visible in the RP images shown in Figs. 7(a) and 7(d). The expected improvement in the microscope resolution obtained by changing the NA_c value from ~0.55 (Fig. 7(b)) to ~0.93 (Fig. 7(e)) can be verified by comparing the zoomed images shown in Figs. 7(c) and 7(f). The periodic Cr structure with p=250 nm is not visible in the image shown in Fig. 7(c) but it is clearly visible in the image shown in Fig. 7(f). This is in correspondence with the values of p_{min} = 270 nm and 224 nm evaluating Eq. (1) for NA_c =0.55 and 0.93, respectively. Both Figures 6 and 7 demonstrates the versatility of the proposed computer-controlled HDC.

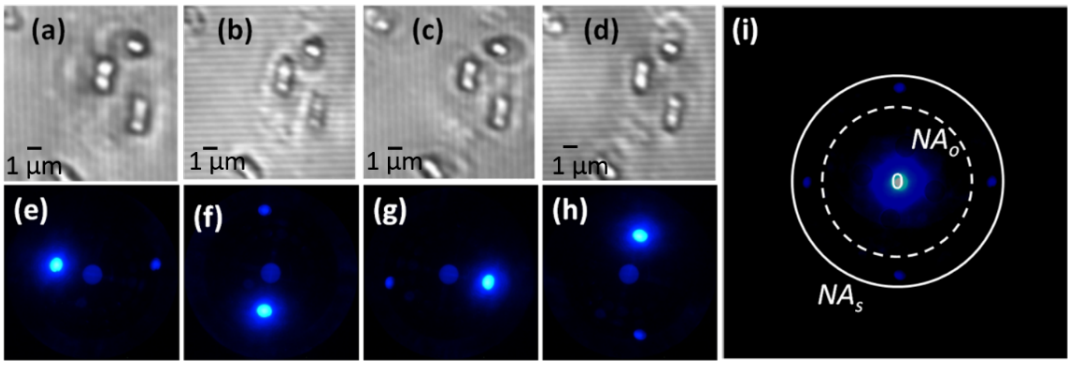

Fig. 8. (a)-(d) RP and (e)-(h) corresponding FP images of E. Coli on top of a Cr pillars array with p=250 nm obtained using the HDC with a single LED in the ON state, a band-pass filter centered at λ=450 nm, and NA_o=1.3. (i) Synthetic FP image with NA_s>NA_o.

Fig. 8 shows images of this sample obtained using the experimental set up sketched in Fig. 1(a), band-pass filter centered at λ=450 nm, and a 100× microscope objective lens with NA_o=1.3. As it is shown in Fig. 8, the sample was imaged turning ON a single LED at the time. Using the same adding shift algorithm described above (Fig. 5), a synthetic FP image could be constructed with $NA_s > NA_c$. A comparison of the synthetic FP images shown in Figs. 5(i) and 8(i) reveals that most of the information of the randomly distributed E. Coli bacteria is contained in the "cloud" around the center of the synthetic FP image. This cloud is formed by superposition of the fuzzy clouds observed around the zero-order diffraction spots in the FP images shown in Figs. 8(e) to 8(h). In the synthetic FP image, the distance between opposite first-order diffraction spots is larger than the diameter of the central cloud because, as

it is seen in the RP images shown in Figs. 8(a) to 8(d), the E. Coli size is larger than the period of the patterned Cr structure.

CHAPTER V
CONCLUSION

The first computer-controlled HDC attached to a common inverted optical microscope are demonstrated in this work. High-resolution images and a variety of both well established and novel optical microscopy techniques were verified with the proposed HDC using periodic patterned samples. In particular, it is proposed to use directly obtained FP images with the HDC, instead of calculating them from RP images, for implementing a new high-resolution microscopy technique, which is a mixture of the FPM and FPIM techniques. Finally, the computer-controlled HDCs are well suited for biomedical imaging applications. An efficient phase recovery algorithm are currently developed to be well fitted for obtaining the optical disturbance at the microscope's FP from the obtained synthetic FP image by following the method proposed in this work.

REFERENCES

1. H. H. Hopkins, and P. M. Barham, "The influence of the condenser on microscopic resolution," Proceeding of the Physical Society, **63**, 737 (1950).
2. H. Köheler, "On Abbe's theory of image formation in the microscope," Optica Acta, **28**, 1691 (1981).
3. A. Vainrub, O. Pustovyy, and V. Vodyanoy, "Resolution of 90 nm (λ/5) in an optical transmission microscope with annular condenser," Opt. Lett. **31**, 2855 (2006).
4. E. Hetcht, Optics (Addison Wesley, Third Edition, 1998).
5. M. Born, and E. Wolf, "Principles of Optics," Pergamon Press, **5**, 1975.
6. J. W. Goodman, "Introduction to Fourier Optics," McGraw-Hill, 1968.
7. L. Molina, D. Dominguez, D. B. Desai, T. O'Loughlin, A. A. Bernussi, and L. Grave de Peralta, "Hemispherical digital optical condensers with no lenses, mirrors, or moving parts," Opt. Express **22**, 6948-6957 (2014).
8. D. B. Desai, D. Dominguez, A. A. Bernussi, and L. Grave de Peralta, "Ultra-thin condensers for optical subwavelength resolution microscopy," J. Appl. Phys. **115**, 093103 (2014).
9. D. Dominguez, M. Alhusain, N. Alharbi, A. Bernussi, and L. Grave de Peralta, "Fourier plane imaging microscopy," J. Appl. Phys. **116**, 103102 (2014).
10. R. Rodriguez, C. J. Regan, A. Ruiz-Columbie, W. Agutu, A. A. Bernussi,and L. Grave de Peralta, "Study of plasmonic crystals using Fourier-plane images obtained with plasmon tomography far-field superlenses," J. Appl. Phys. **110**, 083109 (2011).
11. R. Lopez-Boada, C. J. Regan, D. Dominguez, A. A. Bernussi, and L. Grave de Peralta, "Fundaments of optical far-field subwavelength resolution based on illumination with surface waves," Opt. Express **21**, 11928 (2013).
12. D. Dominguez, S. Sen, N. Fleitas, A. A. Bernussi, and L. Grave de Peralta, "High resolution optical microscopy using far-field illumination produced by plasmonic ultrathin condensers," Biomed. Opt. Express (under review, 2014).
13. D. Dominguez, M. Alhusain, N. Alharbi, A. A. Bernussi, and L. Grave de Peralta, "Fourier plane imaging microscopy for detection of plasmonic crystals with periods beyond the optical diffraction limit," Plasmonic (under review, 2014).
14. G. Zheng C. Kolner, and C. Yang, "Microscopy refocusing and dark-field imaging by using a simple LED array," Opt. Lett. **36**, 3987 (2011).
15. G. Zheng, R. Horstmeyer, and C. Yang, "Wide-field, high-resolution Fourier ptychographic microscopy;" Nature Photonics **7**, 739 (2013).
16. L. Tian, X. Li, K. Ramchandran, and L. Waller, "Multiplexed coded illumination for Fourier ptychography with LED array microscope," Biomed. Opt. Express **14**, 3093 (2014).
17. S. O. Isikman, W. Bishara, S. Mavandadi, F. W. Yu, S. Feng, R. Lau, and A. Ozcan, "Lensfree optical tomographic microscope with a large imaging volumen in a chip," Proc. Nat. Acad. Sci, **18**, 7296 (2011).

18. T. W. Su, S. O. Isikman, W. Bishara, D. Tseng, A. Erlinger, and A. Ozcan, "Multiple-angle lensless digital holography for depth resolved imaging on a chip " Opt. Express, **18**, 9690 (2010).
19. LJ Technologies, 1041 E 24 St, Hialeah, Fl 331013, USA.
20. Z. Liu, L. Tian, S. Liu, and L. Waller, "Real-time brightfield, darkfield, and phase contrast imaging in a light-emitting diode array microscope," J. Biomed. Opt, **19**, 106002 (2014).
21. L. Tian, J. Wang, and L. Waller, "3D differential phase-contrast microscopy with computational illumination using and LED array," Opt. Lett. **39**, 1326 (2014).
22. S. A. Alexandrov, T. R. Hillman, T. Gutzler, and D. D. Sampson, "Synthetic aperture Fourier holographic optical microscopy," Phys. Rev. Lett. **97**, 168102 (2006).
23. D. J. Lee and A. M. Weiner, "Optical phase imaging using a synthetic aperture phase retrieval technique," Opt. Express 22, 9380 (2014).
24. L. Grave de Peralta, C. J. Regan, and A. A. Bernussi, "SPP tomography: a simple wide-field nanoscope," Scanning **35**, 246-252 (2013).
25. S. Dong, P. Nanda, R. Shiradkar, K. Guo, and G. Zheng, "High-resolution fluorescence imaging via pattern-illuminated Fourier Ptychography" Opt. Exp. **22**, 20857 (2014).
26. Fienup, J. R., "Reconstruction of an object from the modulus of its Fourier transform'" Opt. let. **3**, 27 (1978).